Rutherford Scattering

Jamison Lahman, Brandon Coleman, Kenny Richely, Joe Pincura, Jacob Williamson, and Taylor Grueser

***Abstract*—Projecting charged alpha particles at a target sample can be used to estimate the charge and cross-sectional area the target element's nuclei. Through the Coulomb potential, the incoming alpha particles can be deflected and scattered accordingly. Using spectroscopy to identify the resulting energy of the incident alpha particles, we were able to identify an elemental composition of the target. We experimentally determined a target composition of 81.53±0.17% gold, 12.15±0.14% silver, and 6.32±0.19% copper which agrees with the theoretical values of 81% gold, 12% silver, and 7% copper. Additionally, we experimentally determined cross-sectional areas which were consistent with the theoretical values when considering all sources of error.**

I. Introduction & Theory

When a charged particle approaches the nucleus of an atom, the Coulomb potential scatters the oncoming particle. The Coulomb potential is responsible for the static electric force that charged particles experience. The Coulomb potential is given by:

$$U(r) = \frac{Z_0 Z_1 e^2}{4\pi\epsilon_0 r}, \tag{1}$$

where Z_0 and Z_1 are the charges of the two particles and r is the separation[1]. Through elastic collisions, the charge and size of various nuclei can be determined. Alpha particles, doubly ionized helium atoms, are directed towards a material. The nucleus of the atoms of the material are much smaller than the atom themselves and of similar charge as the alpha particle which produces an opportunity for scattering, though it is a small chance. Luckily, many atoms are packed tightly together in material making collisions common enough to observe.

The theoretical Rutherford cross-section is given by the following equation:

$$\frac{d\sigma}{d\Omega} = 1.296 \left(\frac{Z_0 Z_1}{E_0}\right)^2 \left[\frac{1}{\sin^4(\theta/2)} - 2\left(\frac{M_0}{M_1}\right)^2\right], \tag{2}$$

where M_0 and M_1 are the particles' respective masses, E_0 is the incident energy, and θ is the laboratory scattering angle. The Rutherford cross-section will be calculable experimentally by the equation[1],

$$\frac{d\sigma}{d\Omega} = \frac{N_{peak}/(1-dt)}{Nn\Delta\Omega}, \tag{3}$$

where N_{peak} is the number of counts in a given peak, dt is the fractional dead time, N is the number of incident alpha particles, n is the number of nuclei per cm^2 given by the equation,

$$n = \frac{6.54 \times 10^{17}}{\cos(\theta_{target})} \text{ atoms/cm}^2. \tag{4}$$

Instructor: Paul King

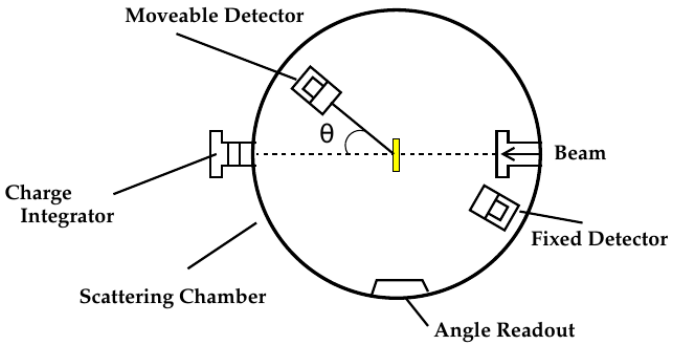

Fig. 1: A simplified schematic of the setup apparatus. The gold foil target is placed at the center of the chamber while two detectors are placed radially around the target. The angles are observed through the angle readout[1].

The solid angle is dependent on the target angle, θ_{target}, rather than the scattering angle. The solid angle is given by the equation,

Because the likelihood of an alpha particle depends on both the number of elemental nuclei as well as the size, the number of counts at each energy position are dependent on these factors. The peak for each element can be related to the other elemental peaks to determine the number of nuclei for each element through the relation,

$$\frac{N_{peak,0}}{N_{peak,1}} = \frac{\sigma_0 n_0}{\sigma_1 n_1}, \tag{5}$$

and σ is the cross-sectional area of the elemental nucleus given by equation (2).

The fractional composition difference between two elements is,

$$\frac{f_0}{f_1} = \frac{n_0/n}{n_1/n} = \frac{n_0}{n_1}. \tag{6}$$

The fractional composition for a given element is therefore,

$$f_i = \frac{n_i}{n_{total}} = \frac{f_i}{\Sigma f} = \frac{1}{1 + \Sigma(f_n/f_i)} \tag{7}$$

with f_n being the fractional composition of element n.

II. Experimental Details

All of the data was collected using Edwards Accelerator Laboratory at Ohio University in Athens, Ohio. Situated at the center of the chamber, shown in Fig. 1, was a target of non-pure gold foil with a composition of approximately 81% gold, 12% silver, and 7% copper. In total, the lab apparatus consisted of two solid-state silicon detectors. A more in-depth experimental design for each detector is given by Fig. 2. The data was collected using DAQ software.

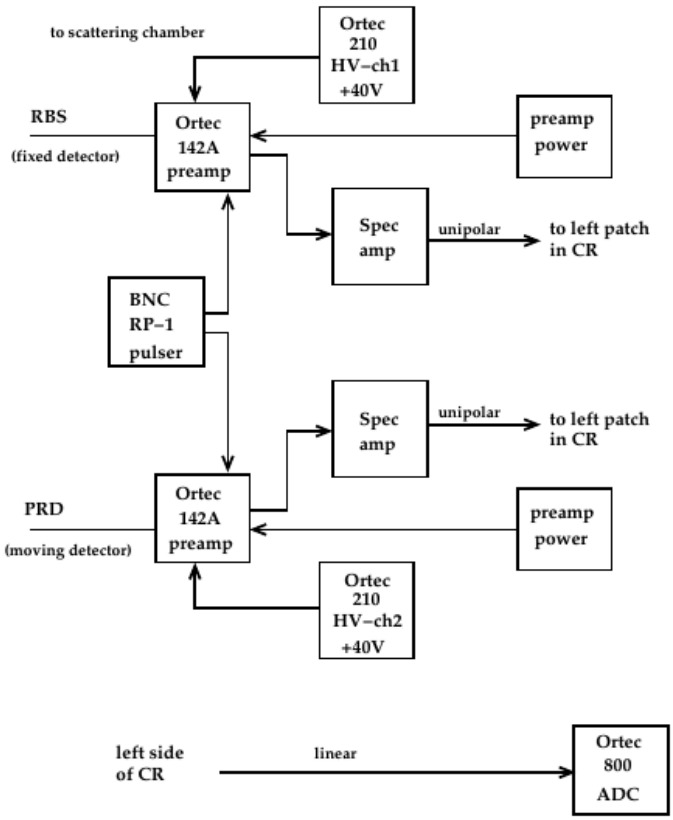

Fig. 2: The total paths from alpha source to detectors then to all necessary amplification before processing using DAQ software[1].

After inspecting the chamber for defects, we measured the dimensions of the apparatus. The aperture of the movable detector was 3.59mm and was 78.00mm from the target. The fixed detector had an aperture of 3.67 and was 63.00mm from the target. In total, we performed 12 experiential runs.

The experiment has four sources of error. In addition to the random error on our peaks, ϵ_N, there is additionally an error on n and the observational error in out angle measurements. The relative errors of the peak counts are both approximately 1% while the error on the angle measurements is estimated to be a few percent. The largest source of error is likely to be on n which is set at 10%. Despite being lower relative errors, the errors on the peaks are the only source of point-to-point errors. ϵ_n and $\epsilon_{\Delta\Omega}$ are both constant throughout the experiment. The total error on σ is given by:

$$\frac{\epsilon_\sigma}{\sigma} = \sqrt{\left(\frac{\epsilon_{N_{peak}}}{N_{peak}}\right)^2 + \left(\frac{\epsilon_N}{N}\right)^2 + \left(\frac{\epsilon_n}{n}\right)^2 + \left(\frac{\epsilon_{\Delta\Omega}}{\Delta\Omega}\right)^2} \quad (8)$$

III. Data

Unfortunately, the accelerator we were using was experiencing technical problems resulting in a lack of high-energy runs. We managed to collect data for one run with 5 MeV alphas. The spectra are plotted in Fig. 3 and 4 while peak analysis is performed in Tab. I and II.

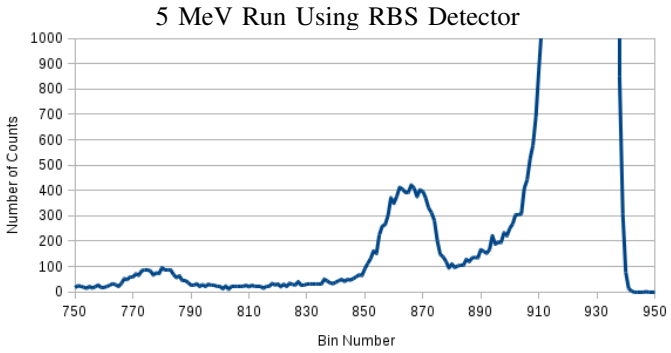

Fig. 3: The spectrum produced by the RBS detector for 5 MeV alpha particles. From left to right, the peaks indicate copper, silver, and gold particles in the target. Scattering due to gold occurred roughly 200 times as often as silver. Much of the gold peak was omitted to show details of the other peaks.

TABLE I: 5 MeV Run Using RBS Detector

Element	N	σ_N	$\bar{x}$	$\sigma_{\bar{x}}$	RMS	f	σ_f
Au	159388	399.23	924.99	0.02	7.07	81.53	0.17
Ag	8393	91.61	864.85	0.08	6.95	12.15	0.14
Cu	1654	40.67	777.61	0.16	6.44	6.32	0.19

Peak analysis of the 5 MeV run using the RBS detector. The concentration of and type of element present in the target are indicated by the position and strength of the peaks. Using the number of peaks along with the theoretical cross-sections, we found fractional compositions for each element following Eq. (7). We determine the target to be $81.53 \pm 0.17\%$ gold, $12.15 \pm 0.14\%$ silver, and $6.32 \pm 0.19\%$ copper.

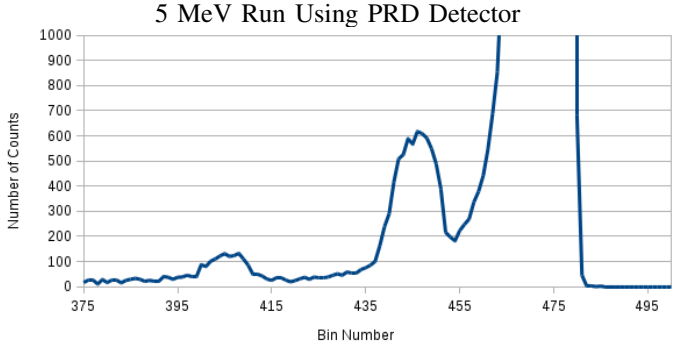

Fig. 4: The spectrum produced by the PRD detector for 5 MeV alpha particles. From left to right, the peaks indicate copper, silver, and gold particles in the target. Scattering due to gold was dominate so the peak was truncated to show details of the other peaks.

TABLE II: 5 MeV Runs Using PRD Detector

Element	N	σ_N	$\bar{x}$	$\sigma_{\bar{x}}$	RMS	f	σ_f
Au	12789	472.73	472.73	0.01	3.75	80.37	0.19
Ag	7391	85.97	445.56	0.05	4.31	13.14	0.16
Cu	1384	37.20	405.71	0.10	3.64	6.49	0.21

Peak analysis of the 5 MeV run using the RBS detector. The concentration of and type of element present in the target are indicated by the position and strength of the peaks. Using the number of peaks along with the theoretical cross-sections, we found fractional compositions for each element following Eq. (7). We determine the target to be $80.37 \pm 0.19\%$ gold, $13.14 \pm 0.16\%$ silver, and $6.49 \pm 0.21\%$ copper.

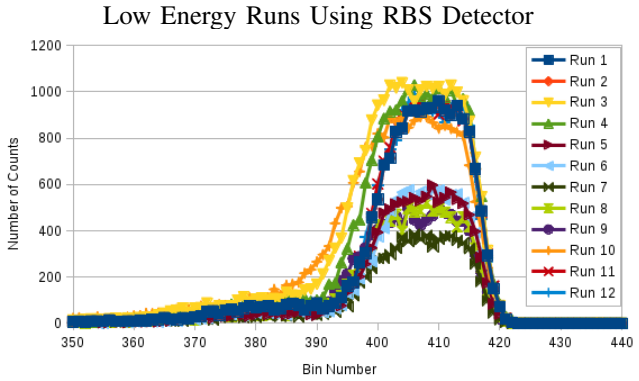

(a) The number of counts and shape of the peaks in the RBS detector are both fairly uniform across runs. This implies there is not a large dependency on the detector angle.

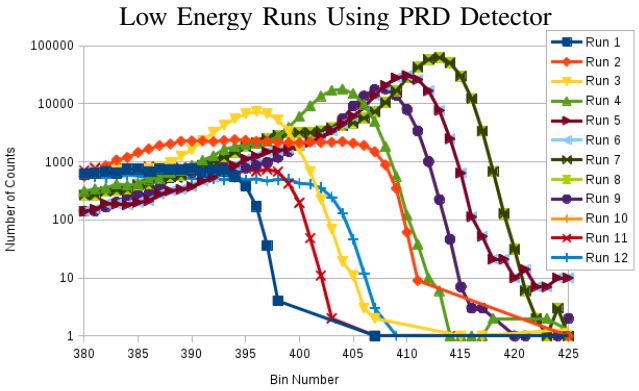

(b) The number of counts and location of the peak in the PRD detector for runs with varying detector angles. The number of counts drastically changes by orders of magnitude suggestion a large angle dependency.

Fig. 5: Low energy runs at various detector angles. As expected, the counts in Fig. 5(a) show the RBS detector is roughly independent of the angle while the counts in Fig. 5(b) shows the PRD has a large angle dependency.

TABLE III: Constant Values for Both Detectors in Low Energy Runs

Run	1	2	3	4	5	6	7	8	9	10	11	12
N_0 (E+12)	3.13	3.13	3.13	3.13	1.69	1.56	1.13	1.56	1.60	3.13	3.13	3.13
ϵ_{N_0} (E+09)	3.13	3.13	3.13	3.13	3.13	3.13	3.13	3.13	3.13	3.13	3.13	3.13
θ_{target} (rad)	0.00	5.50	0.79	0.61	0.44	0.35	5.93	5.89	5.76	5.59	0.00	0.00
$\theta_{detector}$ (rad)	2.44	1.57	1.57	1.22	0.87	0.70	5.59	5.50	5.24	4.89	4.19	4.54
n (E+17/cm^2)	6.54	9.25	9.25	7.98	7.22	6.96	6.96	7.08	7.55	8.54	6.54	6.54
ϵ_n (E+16/cm^2)	6.54	9.25	9.25	7.98	7.22	6.96	6.96	7.08	7.55	8.54	6.54	6.54

TABLE IV: Low Energy Runs Using RBS Detector

Run	1	2	3	4	5	6	7	8	9	10	11	12
N	18844	24633	25543	22987	11857	11857	8133	11069	11462	23471	19413	19210
σ_N	137	157	160	152	109	109	90	105	107	153	139	139
$\bar{x}$	404.36	398.60	401.42	402.63	403.37	403.57	402.32	402.37	401.39	399.86	403.77	403.81
$\sigma_{\bar{x}}$	0.09	0.10	0.09	0.09	0.13	0.13	0.17	0.14	0.14	0.10	0.10	010
dt (%)	1.15	1.41	1.49	1.38	0.65	0.18	0.16	0.64	0.63	1.33	1.00	1.01
$\Delta\Omega$ (E-03 sr)	2.69	2.69	2.69	2.69	2.69	2.69	2.69	2.69	2.69	2.69	2.69	2.69
$\epsilon_{\Delta\Omega}$ (E-05 sr)	5.18	5.18	5.18	5.18	5.18	5.18	5.18	5.18	5.18	5.18	5.18	5.18
σ (E-24 cm^2)	3.46	3.21	3.33	3.47	3.64	4.05	3.84	3.74	3.54	3.31	3.56	3.52
PW Error (E-25 cm^2)	0.37	0.54	0.55	0.96	3.2	7.0	10	5.2	2.1	0.72	0.44	0.53
Total Error (E-24 cm^2)	0.46	1.3	1.3	3.2	1.1	28	32	19	6.1	2.1	0.64	9.2
Residual (E-24 cm^2)	2.41	1.69	1.25	2.64	3.95	7.57	5.27	4.87	2.82	8.63	3.24	2.85
% Error	7.61	0.54	3.95	8.35	12.50	23.93	16.66	15.40	8.92	2.73	9.91	8.99

Data from the low energy runs using the RBS. Dead time is the dead time right. The residuals are calculated using the theoretical value from Eq. (2) which were $\sigma_{au} = 3.67 \times 10^{-24}$cm^2, $\sigma_{ag} = 1.30 \times 10^{-24}$cm^2, and $\sigma_{au} = 4.91 \times 10^{-25}$cm^2. Multiplying the cross-sections by the theoretical, relative abundances in the target, the total cross-section is estimated to be $\sigma = 3.16 \times 10^{-24}$cm^2.

IV. Results

Out estimated composition of $81.53 \pm 0.17\%$ gold, $12.15 \pm 0.14\%$ silver, and $6.32 \pm 0.19\%$ copper from the RBS and $80.37 \pm 0.19\%$ gold, $13.14 \pm 0.16\%$ silver, and $6.49 \pm 0.21\%$ copper from the PRD agree nicely with the hypothesized composition of approximately 81% gold, 12% silver, and 7% copper.

For the low energy runs, our observed data was in agreement theoretical values when all sources of error were taken into account. Considering only point wise error, as seen in Fig. 6a and 6b, the agreement is lost, particularly in regards to the RBS data. Nevertheless, the cross-section in the PRD has an obvious detector angle dependency.

V. Conclusion

We experimentally determined a target composition of $81.53 \pm 0.17\%$ gold, $12.15 \pm 0.14\%$ silver, and $6.32 \pm 0.19\%$ copper as well as $80.37 \pm 0.19\%$ gold, $13.14 \pm 0.16\%$ silver, and $6.49 \pm 0.21\%$ copper, both of which agree with the theoretical values of 81% gold, 12% silver, and 7% copper. Additionally, we experimentally determined cross-sectional areas which were consistent with the theoretical values, however when only considering the piece wise errors, this agreement vanishes. Because of this, we are confident concluding that, through

TABLE V: Low Energy Runs Using PRD Detector

Run	1	2	3	4	5	6	7	8	9	10	11	12
N	15292	59688	61340	122839	190580	455843	378242	290580	11350	86462	21230	30273
σ_N	124	244	248	350	437	675	615	544	337	294	146	174
$\bar{x}$	383.07	392.50	392.18	400.92	407.61	409.44	409.91	409.22	405.16	397.87	384.30	370.68
$\sigma_{\bar{x}}$	0.07	0.05	0.03	0.02	0.01	0.01	0.01	0.01	0.02	0.02	0.07	012
dt (%)	0.92	3.80	3.40	7.02	13.48	10.65	7.65	15.43	6.15	4.59	1.20	2.22
$\Delta\Omega$ (E-03 sr)	1.66	1.66	1.66	1.66	1.66	1.66	1.66	1.66	1.66	1.66	1.66	1.66
$\epsilon_{\Delta\Omega}$ (E-05 sr)	2.3	2.3	2.3	2.3	2.3	2.3	2.3	2.3	2.3	2.3	2.3	2.3
σ (E-24 cm^2)	4.54	12.9	13.2	31.8	109	282	313	190	6.02	20.4	36.32	9.11
PW Error (E-26 cm^2)	3.7	5.4	5.5	9.6	32	70	100	52	21	7.2	4.4	5.3
Total Error (E-24 cm^2)	0.46	1.3	1.3	3.2	1.1	28	32	19	6.1	2.1	6.4	9.2
σ_{theory} (E-24 cm^2)	4.22	13.2	13.2	30.4	103	241	154	52.7	19.3	5.86	9.57	2.85
Residual (E-24 cm^2)	-0.32	-0.27	-0.03	-1.39	-103	-241	-241	-154	-52.7	-19.3	-5.86	-9.57
% Error	-7.48	-2.08	-0.21	-4.55	-5.26	-17.10	-29.85	-23.71	-14.11	-5.79	-7.93	4.81

Data from the low energy runs using the RBS. Dead time is the dead time left. The residuals are calculated using the theoretical value from Eq. (2).

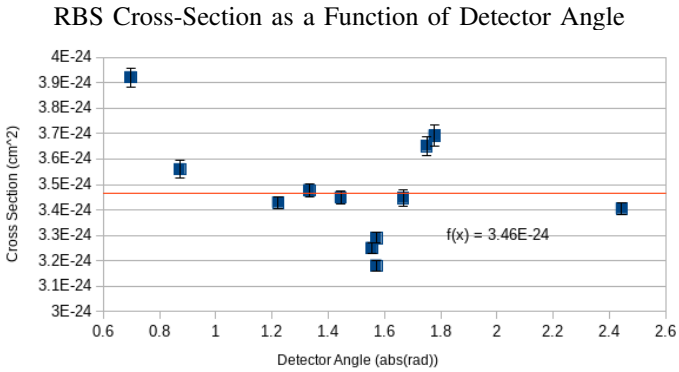

(a) As we expected, the theoretical cross-section is constant for all back scattering.

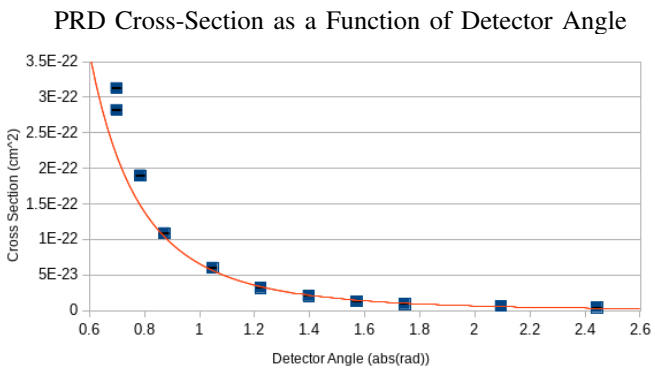

(b) As we expected, the theoretical cross-section is highly dependent on the detector angle.

Fig. 6: The red curve indicates the theoretical cross-section given by the Eq. 2. The points were determined using Eq. 3.

elastic collisions, the charge and size of various nuclei can be experimentally determined.

VI. Acknowledgments

I would like to thank my lab partners: Brandon Coleman, Kenny Richely, Joe Pincura, Jacob Williamson, and Taylor Grueser who helped with the setup, data acquisition and analysis for this report.

References

[1]"Rutherford scattering", Introductory Laboratory – Nucleons.